UNIVERSITY
OF TRENTO

DEPARTMENT OF INFORMATION AND COMMUNICATION TECHNOLOGY

38050 Povo – Trento (Italy), Via Sommarive 14
http://www.dit.unitn.it

MICROWAVE MEDICAL IMAGING: POTENTIALITIES AND LIMITATIONS OF A STOCHASTIC OPTIMIZATION TECHNIQUE

Salvatore Caorsi, Andrea Massa, Matteo Pastorino, and Andrea Rosani

August 2004

Technical Report DIT-04-079

Microwave Medical Imaging: Potentialities and Limitations of a Stochastic Optimization Technique

Salvatore Caorsi*, *Member*, *IEEE*, Andrea Massa**, *Member*, *IEEE*, Matteo Pastorino***, *Senior Member*, *IEEE*, and Andrea Rosani**

* Department of Electronics,

University of Pavia, Via Ferrata 1, 27100 Pavia - Italy

Tel. +39 0382 505661, Fax +39 0382 422583, E-mail: *caorsi@ele.unipv.it*

** Department of Information and Communication Technologies,

University of Trento, Via Sommarive 14, 38050 Trento - Italy

Tel. +39 0461 882057, Fax +39 0461 882093, E-mail: *andrea.massa@ing.unitn.it*

*** Department of Biophysical and Electronic Engineering,

University of Genoa, Via Opera Pia 11/A, 16145 Genoa - Italy

Tel. +39 010 3532242, Fax +39 010 3532245, E-mail: *pastorino@dibe.unige.it*

Microwave Medical Imaging: Potentialities and Limitations of a Stochastic Optimization Technique

Salvatore Caorsi, *Member*, *IEEE*, Andrea Massa, *Member*, *IEEE*, Matteo Pastorino, *Senior Member*, *IEEE*, and Andrea Rosani

Abstract

An approach based on a stochastic optimization technique is proposed for medical microwave imaging. The approach is based on the integral equations of the electromagnetic inverse scattering. After discretization of the continuous model, the problem solution is recast as a global optimization problem. A functional is constructed on the basis of a Markov random field model and minimized by a genetic algorithm. In order to reduce the computational load, a model of the cross section of the biological body is considered. In this way, the investigation area is limited by separating the scattering contribution of a fixed region under test from those of other parts of the model. Some preliminary results concerning a two-dimensional model of a human thorax are reported. Such a biological structure is inspected by the proposed tomographic approach in order to detect and localize the presence of an "object" modeling a tumor.

Key words:

Microwave Imaging, Medical Imaging, Inverse Scattering, Genetic Algorithms, Optimization Problems.

1 Introduction

When the pioneering work by Larsen and Jacobi appeared in 1986 [1], it seemed that techniques based on interrogating microwaves would have provided new and powerful tools for medical diagnostics. However, one should compare the related developments with those of the computerized tomography (CT) in the medical field. In the 70s, the Radon transform was re-discovered and a new era in diagnostic radiology was heralded [2][3]. In fact, few years later, tomographs were already available in several advanced diagnostic units of important hospitals, and, about ten years later, CT has become a routine diagnostic method.

On the contrary, microwave medical imaging is still considered an "emerging" technique and effective dielectric reconstructions are very difficult to be obtained. However, some quite interesting results, including clinical experimentations, have been recently obtained in the case of breast diagnosis by using focusing techniques [4]-[10]. In the authors' opinion, some of the factors that have limited the real capability of microwave medical imaging tend now to reduce their impact on the development of imaging systems. The first aspect concerns the design and realization of efficient illumination/measurement systems. Several equipments have been recently developed, which are based both on arrays of probes [11] and on measurement cameras with advanced sensor matrices [12][13]. The modulated scattering technique [14] has been efficiently applied as well. Consequently, the fast and accurate acquisition of samples of the scattered electromagnetic field is now a feasible task.

Furthermore, as far as the other critical point is concerned, that is the development of effective and accurate inversion procedures, significant advances can be registered. Beside the aforementioned focused approaches, which so far have achieved the best results for breast cancers, other inversion procedures are now sufficiently tested to be considered as potential tools in medical applications. Among them, in the present paper, the authors consider global optimization procedures [15]-[18]. The immediate advantage of

these techniques is related to their capabilities of finding the global minimum of a given functional. Since the inverse scattering problem (which represents the basis theory of microwave imaging techniques) is usually very ill-conditioned and highly nonlinear, the global minimum corresponds to the "exact" solution, whereas a local minimum is related to a "false" solution or an "artifact".

The price to be paid for having the global solution is, as it is well known, a higher computational load. However, in the authors' opinion, modern computers and future computing structures with suitable designed software tools, will make it possible a quasi real time imaging, also in the case in which the usually considered time-consuming optimization techniques are applied. In order to achieve this result, the key points are: (1) hybridization of the stochastic procedure with fast deterministic techniques and (2) capability of inserting *a-priori* information into the model.

In this paper, a stochastic optimization technique is proposed. The approach is based on a hybrid genetic algorithm. In order to reduce the computational load, the method is aimed at separating the scattering effect of the region under consideration (which is usually a limited region of the whole body) from the surrounding tissues. It requires an off-line computation of the Green's matrix and the solution of a forward scattering problem for each reference-tissues distribution. Then a reduced investigation region (which represents the difference between the actual biological structure and the reference-tissues profile) can be considered for a very fast biomedical diagnostics.

The proposed approach, developed for a two-dimensional cross section under transverse magnetic illumination conditions, recasts the inverse problem as an optimization one where a cost function is defined and successively minimized. The cost function is not arbitrarily constructed. Following an approach previously developed in [22], it is obtained by modeling the unknown structure with a Markov random field.

The paper is organized as following. In Section 2, the mathematical formulation of the inverse scattering problem is described, including the separation of the scattering contributions and the construction of the cost function. In Section 3, the hybrid procedure

based on a customized hybrid-coded genetic algorithm is briefly described. Section 4 presents some preliminary results and final conclusions follow (Section 5).

2 Mathematical Formulation

Let us consider Figure 1(a). The cross section of a biological body S, belonging to a square region S_I, is represented by the distributions of the dielectric parameters (e.g., relative dielectric permittivity, ε_r, and electric conductivity, σ [S/m]). Biological tissues are non-magnetic, so that $\mu = \mu_0$ everywhere. When inspected by microwaves, an incident field (transverse-magnetic polarized) is generated and propagated toward the body. Unlike the x-rays, microwaves do not propagate with rectilinear paths. On the contrary, they are scattered in a complex way. If focusing techniques [4]-[10][23] are not used, the whole cross section should be discretized. A large discretization cannot be used due to the high computational load. Moreover, it would require a CPU time not yet compatible with times reasonably expected for real diagnoses in medical applications. It has been shown in [23] that some regions of the body cross section, which are far from the investigated zone, can be neglected. But, it is quite difficult to define the negligible zone and evaluate the errors on the reconstructed values introduced by this strong approximation.

However, a different approach is followed here. Let us consider: $S_I = \bigcup_{n=1}^{N_t} S_n$, where S_n indicates the area of the n-th partition of S_I where the dielectric characteristics are assumed to be constant as well as the field values. Let $\mathbf{s}_n = (x_n, y_n)$ be the center of the n-th partition whose side length is chosen according to the criterion defined in [21]. Moreover, let us assume that only the first N subdomains belong to the investigation area, $S_{ind} = \bigcup_{n=1}^{N} S_n$. Such an area may exhibit dielectric parameters that represent variations of arbitrary fixed values:

$$\widetilde{\varepsilon}\,(x_n, y_n) = \Delta\widetilde{\varepsilon}\,(x_n, y_n) + \widetilde{\varepsilon}^{T}\,(x_n, y_n) \qquad n = 1, ..., N \tag{1}$$

where $\widetilde{\varepsilon}^T$ denotes an arbitrary dielectric value (related to reference biological tissues). Moreover, the other subdomains belonging to the scatterer cross-section S are characterized by $\widetilde{\varepsilon}^H(x_n, y_n)$ $n = (N+1), ..., N_t$. In the above formulas, complex dielectric permittivities are used (i.e., $\widetilde{\varepsilon}(x,y) = \varepsilon_r(x,y) - j\frac{\sigma(x,y)}{2\pi f \varepsilon_0}$).

For the "object" constituted by $\Delta\widetilde{\varepsilon}(x_n, y_n)$, $n = 1, ..., N$, the propagation medium is an inhomogeneous medium (Fig. $1(b)$) characterized by a complex permittivity $\widetilde{\varepsilon}^B(x_n, y_n)$ given by

$$\widetilde{\varepsilon}^B(x_n, y_n) = \begin{cases} \widetilde{\varepsilon}^T(x_n, y_n) & (x_n, y_n) \in S, \qquad n = 1, ..., N \\ \widetilde{\varepsilon}^H(x_n, y_n) & (x_n, y_n) \in S, \quad n = (N+1), ..., N_t \\ \widetilde{\varepsilon}^O(x_n, y_n) & (x, y) \notin S, \qquad (x, y) \in S_I \end{cases} \tag{2}$$

Consequently, the samples of the scattered electric field measured at M locations outside S_I, $(x_m, y_m) \in S_{oss}$, $m = 1, ..., M$, can be related to $\Delta\widetilde{\varepsilon}(x_n, y_n)$ by means of the following scalar Fredholm equation [19]

$$\Psi^{scatt}(x_m, y_m) = \sum_{n=1}^{N} \left\{ [\Delta\widetilde{\varepsilon}(x_n, y_n) - 1] \int\int_{S_n} \Psi^{tot}(x, y)\, \Gamma(x_m, y_m \,|\, x\,,\, y)\, dx\, dy \right\} \tag{3}$$

where $\Psi^{scatt} = \Psi^{tot} - \Psi^{inc}$, Ψ^{tot}, and Ψ^{inc} denote the scattered, total and background fields, respectively; $\Gamma(x,\, y \,|\, x'\,,\, y')$ is the solution of the integral equation [20] below

$$\Gamma(x,\, y \,|\, x'\,,\, y') = \Gamma^O(x,\, y \,|\, x'\,,\, y') + \int\int_{S_I} \left[\widetilde{\varepsilon}^B(x",\, y") - 1\right] \Gamma(x",\, y" \,|\, x'\,,\, y')\, \Gamma^O(x,\, y \,|\, x"\,,\, y")\, dx"\, dy" \tag{4}$$

where Γ^O is the two-dimensional Green's function for free space. Since Γ does not depend on $\Delta\widetilde{\varepsilon}$, for any different reference scenario (i.e., without the "object"), it can be computed

once off-line by means of the Richmond's procedure [24] (as in the present approach) or alternatively by using other numerical procedures. Moreover, it should be noted that such a computation is essentially that of a forward scattering problem, for which fast and efficient direct numerical methods [25] exist.

Once Γ is known, it possible to take into account also the EFIE for the internal field

$$\Psi^{inc}(x_n, y_n) = \Psi^{tot}(x_n, y_n) - \sum_{p=1}^{N} \left\{ [\Delta\widetilde{\varepsilon}(x_p, y_p) - 1] \int\int_{S_p} \Psi^{tot}(x, y)\, \Gamma(x_n, y_n \mid x\,,\, y)\, dx\, dy \right\} \quad (x_n, y_n) \in S \tag{5}$$

From Eqs. (3) and (5), an optimization process can be defined in order to overcome the ill-conditioning (already reduced by the limited discretization). Usually, the cost function to be minimized is arbitrarily chosen. In this paper, the cost function is defined according to a Bayesian approach where the analytical counterparts of $\Delta\widetilde{\varepsilon}$ and Ψ^{tot} are assumed to be the results of spatial stochastic processes. Then, the problem is that of maximizing the *a-posteriori* probability, $Pr\{\Psi^{tot}(x_n, y_n), \Delta\widetilde{\varepsilon}(x_n, y_n) \mid \Psi^{scatt}(x_m, y_m), \Psi^{inc}(x_m, y_m)\}$, $n = 1, ..., N$, $m = 1, ..., M$. By the Bayes theorem, the *a-posteriori* probability can be related to the *a-priori* probability as follows

$$Pr\{\Psi^{tot}(x_n, y_n), \Delta\widetilde{\varepsilon}(x_n, y_n) \mid \Psi^{scatt}(x_m, y_m), \Psi^{inc}(x_m, y_m)\} = \frac{Pr\left\{\Psi^{scatt}(x_m, y_m), \Psi^{inc}(x_m, y_m) \mid \Psi^{tot}(x_n, y_n), \Delta\widetilde{\varepsilon}(x_n, y_n)\right\} Pr\left\{\Psi^{tot}(x_n, y_n), \Delta\widetilde{\varepsilon}(x_n, y_n)\right\}}{Pr\{\Psi^{scatt}(x_m, y_m), \Psi^{inc}(x_m, y_m)\}} \tag{6}$$

Since $Pr\{\Psi^{scatt}(x_m, y_m), \Psi^{inc}(x_m, y_m)\}$ does not contribute to the maximization process, suitable models for $\Delta\widetilde{\varepsilon}(x_n, y_n)$ and $\Psi^{tot}(x_n, y_n)$, $n = 1, ..., N$ are needed. Following the approach proposed in [22][26] and assuming that $\Delta\widetilde{\varepsilon}(x_n, y_n)$ and $\Psi^{tot}(x_n, y_n)$, $n = 1, ..., N$ be described by means of discrete Markov random fields, the maximization of (6) requires to minimize the cost function (also called "energy function")

$$U\left\{\Delta\widetilde{\varepsilon}\left(x_n,y_n\right),\Psi^{tot}\left(x_n,y_n\right);\ n=1,...,N\right\}=\alpha\sum_{n=1}^{N}\sum_{j_n=1}^{J_n}\left|\Delta\widetilde{\varepsilon}\left(x_n,y_n\right)-\Delta\widetilde{\varepsilon}\left(x_{j_n},y_{j_n}\right)\right|^2+$$
$$\beta\sum_{n=1}^{N}\left|\Psi^{tot}\left(x_n,y_n\right)-\Psi^{inc}\left(x_n,y_n\right)-\sum_{p=1}^{N}\left\{\left[\Delta\widetilde{\varepsilon}\left(x_p,y_p\right)-1\right]\int\int_{S_p}\Psi^{tot}\left(x,y\right)\Gamma\left(x_n,y_n\,|\,x\ ,\ y\right)dx\,dy\right\}\right|^2+$$
$$\gamma\sum_{m=1}^{M}\left|\Psi^{scatt}\left(x_m,y_m\right)-\sum_{n=1}^{N}\left\{\left[\Delta\widetilde{\varepsilon}\left(x_n,y_n\right)-1\right]\int\int_{S_n}\Psi^{tot}\left(x,y\right)\Gamma\left(x_m,y_m\,|\,x\ ,\ y\right)dx\,dy\right\}\right|^2 \tag{7}$$

where the summation over j_n extends to the neighborhood subdomains of the n-th subdomain; $\alpha=\frac{1}{\sum_{n=1}^{N}\sum_{j_n=1}^{J_n}\left|\widetilde{\varepsilon}^T(x_n,y_n)-\widetilde{\varepsilon}^T(x_{j_n},y_{j_n})\right|^2}$, $\beta=\frac{1}{\sum_{n=1}^{N}\left|\Psi^{inc}(x_n,y_n)\right|^2}$, and $\gamma=\frac{1}{\sum_{m=1}^{M}\left|\Psi^{scatt}(x_m,y_m)\right|^2}$. In this way, the cost function is defined according to an assumption on the model and it is not arbitrarily constructed. It should be noted that the procedure for obtaining (7) is the same as proposed in [22], although the integral equations are completely different and customized for the problem at hand. Moreover, Eq. (7) is solved here by means of an evolutionary algorithm, which is much more efficient that a stochastic single-agent procedure (as the "sequential" simulated annealing) used in [22].

3 Optimization Procedure

3.1 "Object" Parameterization

In order to further reduce the computational load of the optimization process, by limiting the search space of the minimization, the investigation area S_{ind} is approximated by a homogeneous square of side L_C and centered at (x_C, y_C). Under this hypothesis, the dielectric differential permittivities of the domains belonging to the investigation area are given by

$$\Delta\widetilde{\varepsilon}\left(x_n,y_n\right)=\begin{cases}\Delta\widetilde{\varepsilon}_{ind} & X,\,Y\in\left[-\frac{L_C}{2},\frac{L_C}{2}\right]\\ 0 & otherwise\end{cases} \tag{8}$$

where $X=(x_n-x_C)\,cos\theta+(y_n-y_C)\,sin\theta$, $Y=(x_C-x_n)\,sin\theta+(y_n-y_C)\,cos\theta$, θ being the "object" orientation. Consequently, the reconstruction process is aimed at searching for the unknown array $\Omega=\{x_C,\ y_C,\ L_C,\ \theta,\ \Delta\widetilde{\varepsilon}_{ind};\ \Psi^{tot}\left(x_n,y_n\right)\ n=1,...,N\}$ minimizing

(7) by considering the parameterization rule defined in (8).

To this end, a suitable Genetic Algorithm (GA) is used to define a sequence of trial configurations, $\Omega^{(k)}$, $k = 1, ..., K_{max}$, (k being the iteration number), which converges to an extreme of the cost function.

3.2 Optimization Procedure

GAs [15]-[17] are efficient optimization techniques that mathematically reproduce the genetic evolution occurring in natural processes. A standard implementation of a GA considers a set of trial solutions $\overline{\Omega}^{(k)} = \left\{\Omega_q^{(k)},\, q = 1, ..., Q\right\}$ (called *population*) coded with a suitable representation $\psi_q^{(k)} = C\left\{\Omega_q^{(k)}\right\}$, $q = 1, ..., Q$ and ranked according to their *fitness* (i.e., the corresponding value of the scalar cost function) $U_q^{(k)} = U\left\{\Omega_q^{(k)}\right\}$, $q = 1, ..., Q$. Iteratively, the population evolves generating new chromosomes, $\widetilde{\psi}_q^{(k)}$(called *offspring*), by means of *crossover* and *mutation* [16]. According to a generational strategy [17], the current population is replaced by the newly generated group of offspring, $\overline{\Omega}^{(k+1)} \Leftarrow \overline{\widetilde{\Omega}}^{(k)}$ where $\overline{\widetilde{\Omega}}^{(k)} = \left\{\widetilde{\Omega}_q^{(k)},\, q = 1, ..., Q\right\}$. The iterative process terminates either if a maximum number of generations elapses ($k = K_{max}$) or a fixed value of the cost function is reached $U_{opt}^{(K^*)} = min_q\left\{U_q^{(K^*)}\right\} \leq \eta$, η being the convergence threshold and $k = K^*$ the convergence iteration.

The first step in adapting a standard GA optimizer to the problem at hand is to choose a suitable coding, or mapping C, of the unknown parameters into genes. Due to the variable dimension of the "object" and the discretization of the investigation domain in square sub-domains (ℓ-sided), the most natural chromosome structure is a two-part variable-length string where each trial solution Ω is coded by using a concatenated multi-parameter scheme $\psi = \{\psi_b, \psi_r;\, b = 1, ..., B;\, r = 1, ..., N\}$. The first part of the chromosome, $\{\psi_b;\, b = 1, ..., B\}$, is related to the "object" characteristics, x_C, y_C, L_C, θ, and $\Delta\widetilde{\varepsilon}_{ind}$ which are coded in fixed-length binary strings. On the contrary, a real-valued variable-length representation, $\{\psi_r;\, r = 1, ..., N\}$, is used for the electric field unknowns, $\Psi^{tot}(x_n, y_n)$. The use of a variable-length structure is necessary due to the variable num-

ber of sub-domains N (determined by L_C) occupied by the "object" where the unknown field should be computed.

As far as the genetic operators are concerned, unlike selection (a *proportionate selection* [17] is adopted) crossover and mutation operates directly on the chromosome themselves. Consequently, it is therefore mandatory to design genetic operators able to fully exploit the adopted representation.

- *Mutation*

  The mutation operator provides a mean for exploring portions of the solution space that are not represented in the genetic complement. If the mutation position lies in the binary part of the chromosome, then the selected bit is changed from zero to one or vice-versa, $\widetilde{\psi}_b = not\,\{\psi_b\}$. Otherwise, mutation is performed by perturbing the randomly chosen *allele*, ψ_r, by an amount $\Delta\psi_r$ chosen from a uniform distribution with zero mean and deviation chosen as 10 % of the gene's range ($\widetilde{\psi}_r = \psi_r + \Delta\psi_r$).

- *Crossover*

  The crossover operations are aimed at rearranging the genetic complement of a population to produce better combinations of genes and more fit solutions. Let us consider two parents $(\psi)_a$ and $(\psi)_b$ selected for the crossover and assume that a *single-point-crossover* [17] be used.

  If the cross-position lies into the binary part of the chromosome and the "object" of the produced offspring occupies a number of sub-domains equal to or smaller than that occupied by one of their parents ($\left(\widetilde{N}\right)_i \leq max_j\,\{N_j\}$, $i, j = a,\, b$), then

$$\begin{aligned} \left\{\widetilde{\Psi}^{tot}\left(x_n, y_n\right)\right\}_a &= \frac{r\left\{\Psi^{tot}(x_n,y_n)\right\}_a + (1-r)\left\{\Psi^{tot}(x_n,y_n)\right\}_b}{2}, \quad n = 1, ..., \left(\widetilde{N}\right)_a \\ \left\{\widetilde{\Psi}^{tot}\left(x_n, y_n\right)\right\}_b &= \frac{(1-r)\left\{\Psi^{tot}(x_n,y_n)\right\}_a + r\left\{\Psi^{tot}(x_n,y_n)\right\}_b}{2}, \quad n = 1, ..., \left(\widetilde{N}\right)_b \end{aligned} \tag{9}$$

where $\left(\widetilde{N}\right)_i = \left\{ int\left[\frac{\left(\widetilde{L_C}\right)_i}{\ell}\right]\right\}^2$ and $r \in [0,1]$ is a random number. Otherwise, if $\left(\widetilde{N}\right)_i > max_j\left\{N_j\right\}$, $i,j = a,\, b$, then

$$\left\{\widetilde{\Psi}^{tot}\left(x_n, y_n\right)\right\}_i = \xi^{tot}\left(x_n, y_n\right),\ n = \left(max_j\left\{N_j\right\}+1\right), ..., \left(\widetilde{N}\right)_i \quad i,\, j = a,\, b \tag{10}$$

ξ^{tot} being the electric field for the configuration without the "object".

Finally, when the cross-position lies into the real part of the chromosome, the alleles are combined to sensibly hybridize population members according to the rule proposed in [27] (pp. 43-44).

4 Numerical Assessment

In order to preliminary assess the potentialities and current limitations of the proposed stochastic optimization technique, let us consider, as a test case, a schematized model of a human thorax where the "object", to be detected and localized (if it exists), models a homogeneous malignant tissue.

The biological phantom is the same as used by Caorsi *et al.* for the evaluation of a focused medical imaging [23]. The biological structure, whose dielectric parameters are shown in Fig. 2, is placed in a homogeneous non-dissipative medium and is illuminated by a set of unit TM plane waves impinging from $V = 4$ different directions ($\theta^v = (v-1)\frac{2\pi}{V}$, $v = 1, ..., V$) at a frequency $f = 433\, MHz$.

The samples of the scattered electric field at the measurement points are obtained by a forward scattering computation with the Richmond's method [24], which has been found to be accurate for the 2D-TM scattering (in most complex cases, other approaches of the computational electromagnetics should be used; e. g., the finite element method or the finite difference method). Moreover, in order to take into account more realistic operation conditions, the simulated scattered data have been corrupted by adding an

additive Gaussian noise with zero mean value and signal-to-noise ratio equal to $SNR = 30\,dB$.

As far as the "object", modeling a tumor, is concerned, three different geometries (Fig. 3) are considered. Moreover, for this preliminary assessment, the dielectric properties of the tumor are assumed to be known. The side of the object is assumed to be $L_C = 0.021\,\lambda$. The object is located at the position $x_C = 0.047\,\lambda$ and $y_C = -0.018\,\lambda$(Fig. $3(a)$), $x_C = -0.097\,\lambda$ and $y_C = 0.105\,\lambda$ (Fig. $3(b)$), and $x_C = 0.119\,\lambda$ and $y_C = -0.033\,\lambda$ (Fig. $3(c)$) in the scenario "kidney", "liver" and "muscle", respectively. The dielectric properties of the malignant tissues are assumed equal to that reported in [29][28]: $\widetilde{\varepsilon}^{kidney} = 58.5 - j34.87$ ($\widetilde{\varepsilon}^{T,kidney} = 62.0 - j37.36$), $\widetilde{\varepsilon}^{liver} = 58.0 - j31.96$ ($\widetilde{\varepsilon}^{T,liver} = 52.5 - j26.15$), and $\widetilde{\varepsilon}^{muscle} = 54.4 - j31.13$ ($\widetilde{\varepsilon}^{T,muscle} = 52.6 - j28.22$).

4.1 Error Figures

In order to give a quantitative indication on the localization accuracy of the proposed approach, the following *object-localization error*, δ_C, is defined:

$$\delta_C = \frac{\sqrt{\left(x_C - \widehat{x}_C\right)^2 + \left(y_C - \widehat{y}_C\right)^2}}{d_{max}} \times 100 \tag{11}$$

where $d_{max} = \sqrt{2}L_S$ (L_S being the side of the square region S) is the maximum error in defining the crack center when it belongs to the host background and where the superscript $\widehat{\ }$ differentiates the reconstructed quantities from actual values.

4.2 Preliminary Results

The first example is aimed at evaluating the detection capabilities of the approach for different dimensions of the schematized tumor with respect to the reference scenarios shown in Fig. 3. The "object" dimensions are changed between $\left(\frac{L_C}{\lambda}\right)^2 = 4.9 \times 10^{-6}$ and $\left(\frac{L_C}{\lambda}\right)^2 = 12.25 \times 10^{-4}$ and the plots of the localization errors are shown in Figure $4(a)$. As can be observed, δ_C is almost constant and equal to about 20 for the case of liver-tumor.

Also the plot related to the "object" inside the muscle tissue presents a similar behavior, but with a large increase of the percentage error (about 25), which produces a very poor localization. As far as the "kidney" scenario is concerned, δ_C shows a monotonic increase in the range between 12 and 38 corresponding to an increasing of the "object" dimensions. An idea about the detection accuracy during the iterative process can be drawn (for $\delta_C = 22$) from Fig. $4(b)$, which shows an image of the evolution of tumor center estimation ($K* = 101$ being the convergence iteration) when the "liver" scenario is considered and for a tumor dimension equal to $\left(\frac{L_C}{\lambda}\right)^2 = 0.5 \times 10^{-4}$.

In the second example, to test the dependence of the localization accuracy on tumor dielectric characteristics, let us consider some variations in the permittivity and conductivity of the "object" ranging from -30% to 30 % of the reference value ($\left\{\widetilde{\varepsilon}^{(i)}\right\}' = \widetilde{\varepsilon}^{(i)} \pm 0.3\,\widetilde{\varepsilon}^{(i)}$, $i = kidney,\ liver,\ muscle$). Figure 5 shows the achieved results (in term of localization errors) when only the dielectric permittivity of the object (Fig. $5(a)$ - $\left\{\varepsilon_r^{(i)}\right\}' = \varepsilon_r^{(i)} \pm 0.3\,\varepsilon_r^{(i)}$ and $\left\{\sigma^{(i)}\right\}' = \sigma^{(i)}$) or its conductivity (Fig. $5(b)$ - $\left\{\sigma^{(i)}\right\}' = \sigma^{(i)} \pm 0.3\,\sigma^{(i)}$ and $\left\{\varepsilon_r^{(i)}\right\}' = \varepsilon_r^{(i)}$) is changed. As can be seen, the "object" location is almost independent of its dielectric permittivity for the "muscle" scenario with an average error equal to $av\{\delta_C\} = 16.5$. The average error slightly increases for the "kidney" scenario ($av\{\delta_C\} = 20.0$) with values ranging between $min\{\delta_C\} = 11.9$ and $max\{\delta_C\} = 25.9$. On the contrary, large oscillations can be observed in the plot related to the "liver" scenario with a wider range of variations $24.7 \leq \delta_C \leq 51.4$. This seems to indicate: (*1*) a good robustness of the method in localizing the "object" for the "muscle" scenario; (*2*) satisfactory performances for the "kidney" test-case, but increasing difficulties for the case of "liver" scenario when the dielectric permittivity of the tumor strongly differs from the reference value ($\varepsilon_r^{(liver)} = 58.0$). As far as conductivity variations of the malignant tissue are concerned, different observations can be carried out. For this example, a more consistent dynamic on δ_C is shown in the "muscle" scenario ($24.4 \leq \delta_C \leq 54.4$) with respect to the variations occurring for the "kidney" ($9.0 \leq \delta_C \leq 23.5$) and "liver" scenarios ($24.4 \leq \delta_C \leq 37.6$) .

For completeness, the influence of variations on the host-tissue is also analyzed. As for

the tumor variations, the localization accuracy is evaluated for different values of the host-tissue relative permittivity or conductivity, as shown in Fig. 6(a) ($\left\{\varepsilon_r^{T(i)}\right\}' = \varepsilon_r^{T(i)} \pm 0.3\,\varepsilon_r^{T(i)}$ and $\left\{\sigma^{T(i)}\right\}' = \sigma^{T(i)}$) and Fig. 6($b$) ($\left\{\sigma^{T(i)}\right\}' = \sigma^{T(i)} \pm 0.3\,\sigma^{T(i)}$ and $\left\{\varepsilon_r^{T(i)}\right\}' = \varepsilon_r^{T(i)}$), respectively. It turns out to be that the localization error is lower than 29% for the "kidney" scenario ($10.8 \leq \delta_C\left(\left\{\varepsilon_r^{T(kidney)}\right\}'\right) \leq 28.5$ and $5.9 \leq \delta_C\left(\left\{\sigma^{T(kidney)}\right\}'\right) \leq 20.1$). Its maximum value increases to 43% for the "liver" scenario ($23.4 \leq \delta_C\left(\left\{\varepsilon_r^{T(liver)}\right\}'\right) \leq 43.0$ and $26.3 \leq \delta_C\left(\left\{\sigma^{T(liver)}\right\}'\right) \leq 38.9$). The threshold value ($\delta_C \cong 62.0$) is achieved for the "muscle" scenario ($23.0 \leq \delta_C\left(\left\{\varepsilon_r^{T(muscle)}\right\}'\right) \leq 49.0$ and $23.6 \leq \delta_C\left(\left\{\sigma^{T(muscle)}\right\}'\right) \leq 62.5$).

5 Conclusions

In this paper an inverse-scattering-based procedure has been proposed for microwave imaging in the biomedical framework. The approach is based on an evolutionary algorithm able to solve the optimization problem arising from the inverse scattering formulation. By separating the scattering contributions of the investigation region and of the remaining part of the biological scatterer cross section, the computational load is strongly reduced. After an off-line forward computation, the imaging process is timely carried out due to the limited discretization. The use of the global optimization procedure still guarantees the global solution, avoiding artifacts and false solution. Moreover, the approach resorts to a model description in terms of Markov random fields, which allows the definition of the cost function to be minimized without arbitrary assumptions.

Preliminary numerical results seems to confirm the effectiveness but also current limitations of the proposed approach. They suggest to consider more extensive investigations in order to define the operating conditions for an accurate imaging (e.g., different working frequencies as well as various illumination conditions). Moreover, since the proposed approach is able to deal with the monitoring of physiological features of the "object", the assessment will be completed by considering not only the localization problem but also

the quantitative reconstruction of the region under test.

On the other hand, the extension of the method to a full three-dimensional configuration represents an important objective of current research activities of the authors' team. The main difficulties are of course related to the computational load. In order to overcome this drawback, a customized parallel implementation of the GA-based procedure is currently under development.

Acknowledgment

The authors wish to express their gratitude to Prof. Paul Meaney for providing them with reference biomedical data.

References

[1] L. E. Larsen and J. H. Jacobi, Eds., *Medical Applications of Microwave Imaging*. New York: IEEE Press, 1986.

[2] G. N. Hounsfield, "Computerized transverse axial scanning (tomography). I. Description of system," *Br. J. Radiol.*, vol. 46, pp. 1016-1024, 1973.

[3] J. F. Greenleaf et *al.*, "Algebraic reconstruction of spatial distributions of acoustic absorption within tissue from their two-dimensional acoustic projections," in *Acoustical Holography*, P. S. Green (Ed.), vol. 5, pp. 591-603, Plenum Press, New York, 1974.

[4] S. K. Moore, "Better breast cancer detection," *IEEE Spectrum*, vol. 38, pp. 50-54, 2001.

[5] E. C. Fear, P. M. Meaney, and M. A. Stuchly, "Microwaves for breast cancer detection?," *IEEE Potentials*, vol. 22, pp. 12-18, 2003.

[6] E. C. Fear, S. C. Hagness, P. M. Meaney, M. Okoniewski, and M. A. Stuchly, "Enhancing breast tumor detection with near-field imaging," *IEEE Microwave Mag.*, vol. 3, pp. 48-56, 2002.

[7] P. M. Meaney, S. A. Pendergrass, M. W. Fanning, D. Li, and K. D. Paulsen, "Importance of using a reduced contrast coupling medium in 2D microwave breast imaging," *J.Electromagnetic Waves Appl.* - Special Issue on "Microwave Imaging and Inverse Scattering Techniques", Eds. A. Massa and S. Caorsi, vol. 17, no. 2, pp. 357-382, 2003.

[8] Z. Q. Zhang and Q. H. Liu, "Microwave imaging for breast tumor: 2D forward and inverse methods," *IEEE Antennas Propagat. Soc. Int. Symp.*, vol. 1, pp. 242-245, 2001.

[9] S. K. Davis, E. J. Bond, X. Li, S. C. Hagness, and B. D. Van Veen, "Imaging via space-time beamforming for early detection of breast cancer: beamformer design in the frequency domain," *J.Electromagnetic Waves Appl.* - Special Issue on "Microwave Imaging and Inverse Scattering Techniques", Eds. A. Massa and S. Caorsi, vol. 17, no. 2, pp. 333-356, 2003.

[10] E. J. Bond, X. Li, S. C. Hagness, and B. D. Van-Veen, "Microwave imaging via space-time beamforming for early detection of breast cancer," *IEEE Trans. Antennas Propagat.*, vol. 51, pp. 1690-1705, 2003.

[11] L. Jofre, M. S. Hawley, A. Broquetas, E. de los Reyes, M. Ferrando, and A. R. Elias-Fuste,"Medical imaging with a microwave tomographic scanner," *IEEE Trans. Biomedical Eng.*, vol. 37, pp. 303-312, 1990.

[12] A. Franchois, A. Joisel, C. Pichot, and J. C. Bolomey, "Quantitative microwave imaging with a 2.45-GHz planar microwave camera," *IEEE Trans. Medical Imaging*, vol. 17, pp. 550-561, 1998.

[13] J. C. Bolomey and C. Pichot, "Microwave tomography: from theory to practical imaging systems", *Int. J. Imaging Systems and Technol.*, vol. 2, pp. 144-156, 1990.

[14] J. C. Bolomey and F. E. Gardiol, *Engineering Applications of the Modulated Scatterer Technique*. Artech House, Norwood, MA, 2001.

[15] R. L. Haupt, "An introduction to genetic algorithms for electromagnetics," *IEEE Antennas Propagat. Mag.*, vol. 37, pp. 7-15, 1995.

[16] D. S. Weile and E. Michielssen, "Genetic algorithm optimization applied to electromagnetics: a review," *IEEE Trans. Antennas Propagat.*, vol. 45, pp. 343-353, 1997.

[17] J. M. Johnson and Y. Rahmat-Samii, "Genetic algorithms in engineering electromagnetics," *IEEE Antennas Propagat. Mag.*, vol. 39, pp. 7-25, 1997.

[18] P. Moscato, "On evolution, search, optimization, genetic algorithms and martial arts towards memetic algorithms," Tech. Rep. Caltech Concurrent Computation Program, no. 826, California Institute of Technology, Pasadena, California, USA, 1989.

[19] D. Colton and R. Kress, *Inverse Acoustic and Electromagnetic Scattering Theory*. Springer, Berlin, 1992.

[20] S. Caorsi, G. L. Gragnani, M. Pastorino, and M. Rebagliati, "A model-driven approach to microwave diagnostics in biomedical applications," *IEEE Trans. Microwave Theory Tech.*, vol. 44, pp. 1910-1920, 1996.

[21] M. J. Hagmann, O. P. Gandhi, and C. H. Durney, "Upper bound on cell size for moment method solutions," *IEEE Trans. Microwave Theory Techn.*, vol. 25, pp. 831-832, 1977.

[22] S. Caorsi, G. L. Gragnani, S. Medicina, M. Pastorino, and G. Zunino, "Microwave imaging based on a Markov random field model", *IEEE Trans. Antennas Propagat.*, vol. 42, pp. 293-303, 1994.

[23] S. Caorsi, A. Massa, and M. Pastorino, "Numerical assessment concerning a focused microwave diagnostic method for medical applications," *IEEE Trans. Microwave Theory Tech.*, Special Issue on "RF/Microwave Applications in Medicine," vol. 48, pp. 1815-1830, 2000.

[24] J. H. Richmond, "Scattering by a dielectric cylinder of arbitrary cross section shape," *IEEE Trans. Antennas Propagat.*, vol. 13, pp. 334-341, 1965.

[25] W. C. Chew, J.-M. Jin, E. Michielssen, and J. Song, *Fast and Efficient Algorithms in Computational Electromagnetics*. Artech House, Norwood, MA, 2001.

[26] S. Geman and D. Geman, "Stochastic relaxation, Gibbs distributions, and the Bayesian restoration of images," *IEEE Trans. Pattern Anal. Machine Intell.*, vol. 6, pp. 721-741, 1984.

[27] D. S. Weile and E. Michielssen, "Genetic algorithms: theory and advanced techniques," in *Electromagnetic Optimization by Genetic Algorithms*, Eds. Y. Rahmat-Samii and E. Michielssen, J. Wiley & Sons, Inc., New York, 1999.

[28] W. T. Joines, Y. Zhang, C. Li, and R. L. Jirtle, "The measured electrical properties of normal and malignant human tissues from 50 to 900 MHz," *Med. Phys.*, vol. 21, pp. 547-550, 1994.

[29] K. R. Foster and J. L. Schepps, "Dielectric properties of tumor and normal tissues at radio through microwave frequencies," *J. Micro. Power*, vol. 16, pp. 107-119, 1981.

FIGURE CAPTIONS

- Figure 1.

  Problem geometry: (a) actual scenario and (b) background medium.

- Figure 2.

  Schematized human thorax. Color-level representation for (a) permittivity, ε_r, and (b) conductivity, $\sigma\,[S/m]$, distributions.

- Figure 3.

  Schematized test-case scenarios. Color-level representation of the dielectric parameters distribution for (a) scenario "kidney", (a) scenario "liver", and (a) scenario "muscle".

- Figure 4.

  Object detection and location - (a) Localization error versus "object" area for different scenarios. (b) Iterative approximation of the "object" location during the stochastic optimization process.

- Figure 5.

  Object detection and location - Localization error versus (a) dielectric permittivity $(0.7\,\varepsilon_r^{(i)} \leq \left\{\varepsilon_r^{(i)}\right\}' \leq 1.3\,\varepsilon_r^{(i)};\ \left\{\sigma^{(i)}\right\}' = \sigma^{(i)})$ and (b) conductivity $(0.7\,\sigma^{(i)} \leq \left\{\sigma^{(i)}\right\}' \leq 1.3\,\sigma^{(i)};\ \left\{\varepsilon_r^{(i)}\right\}' = \varepsilon_r^{(i)})$ of the "object" and for different scenarios.

- Figure 6.

  Object detection and location - Localization error versus (a) dielectric permittivity $(0.7\,\varepsilon_r^{T(i)} \leq \left\{\varepsilon_r^{T(i)}\right\}' \leq 1.3\,\varepsilon_r^{T(i)};\ \left\{\sigma^{T(i)}\right\}' = \sigma^{T(i)})$ and (b) conductivity $(0.7\,\sigma^{T(i)} \leq \left\{\sigma^{T(i)}\right\}' \leq 1.3\,\sigma^{T(i)};\ \left\{\varepsilon_r^{T(i)}\right\}' = \varepsilon_r^{T(i)})$ of the "host-tissue" and for different scenarios.

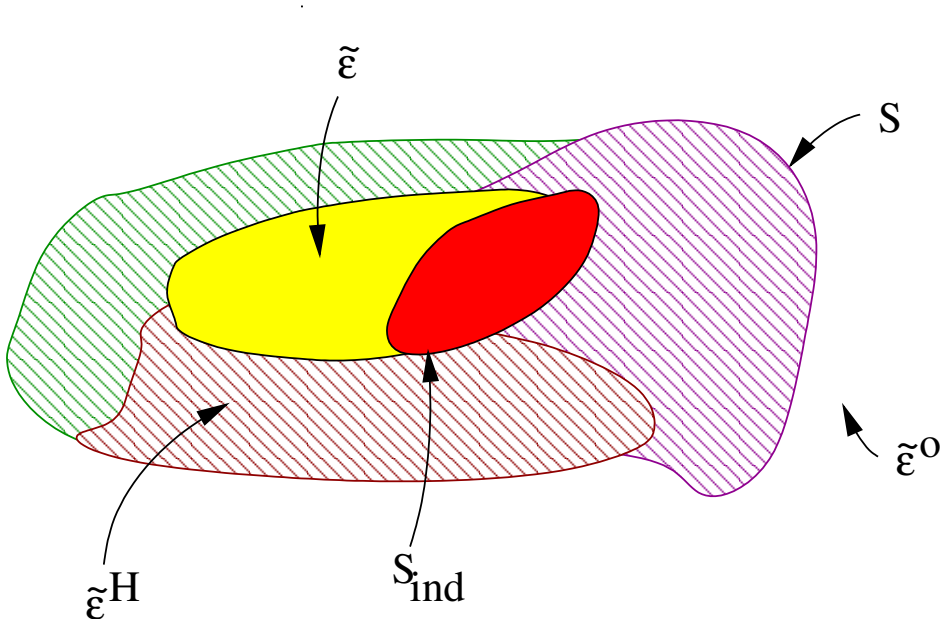

(*a*)

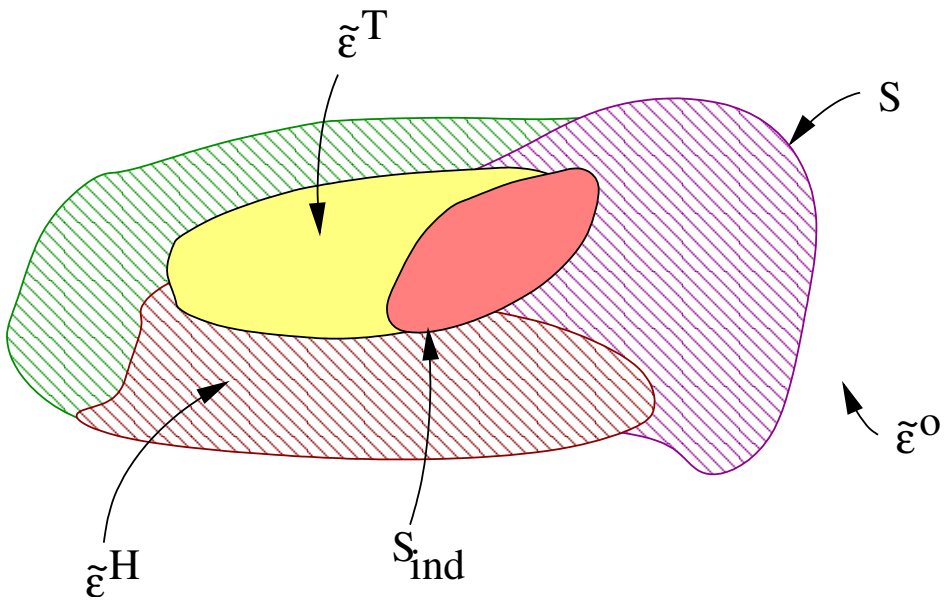

(*b*)

Fig. 1 - S. Caorsi *et al.*, "Microwave medical imaging: potentialities ..."

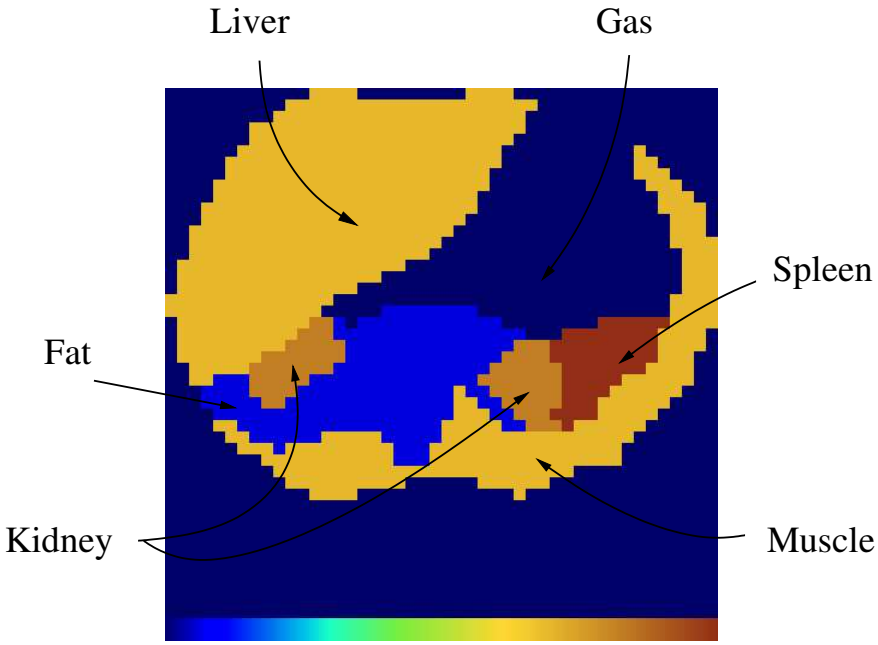

(a)

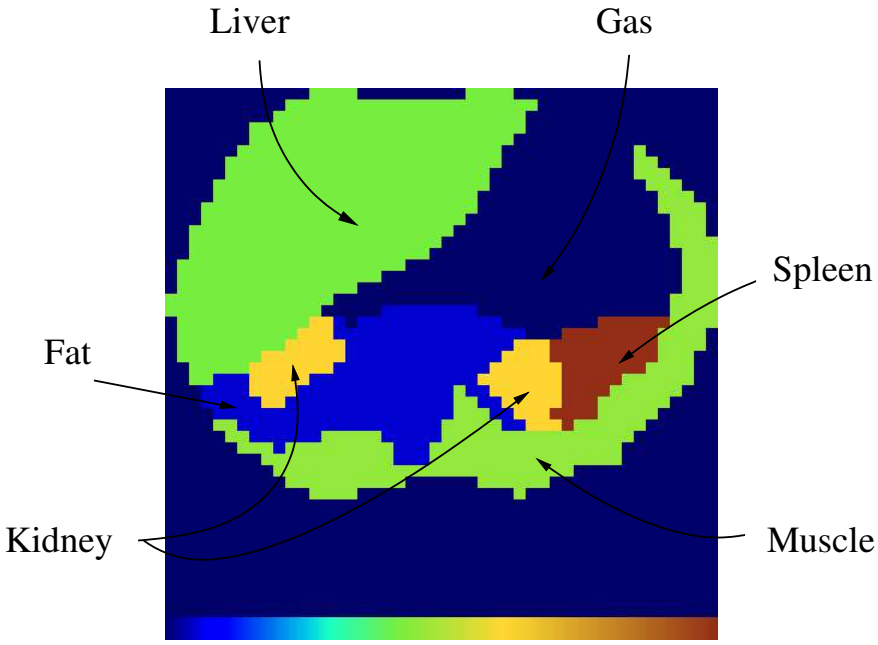

(b)

Fig. 2 - S. Caorsi *et al.*, "Microwave medical imaging: potentialities ..."

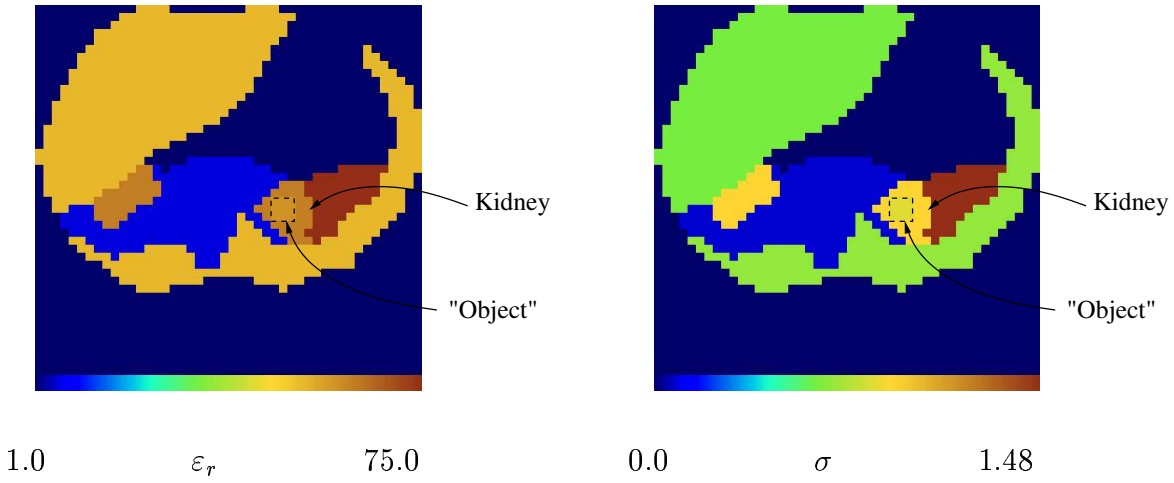

(a)

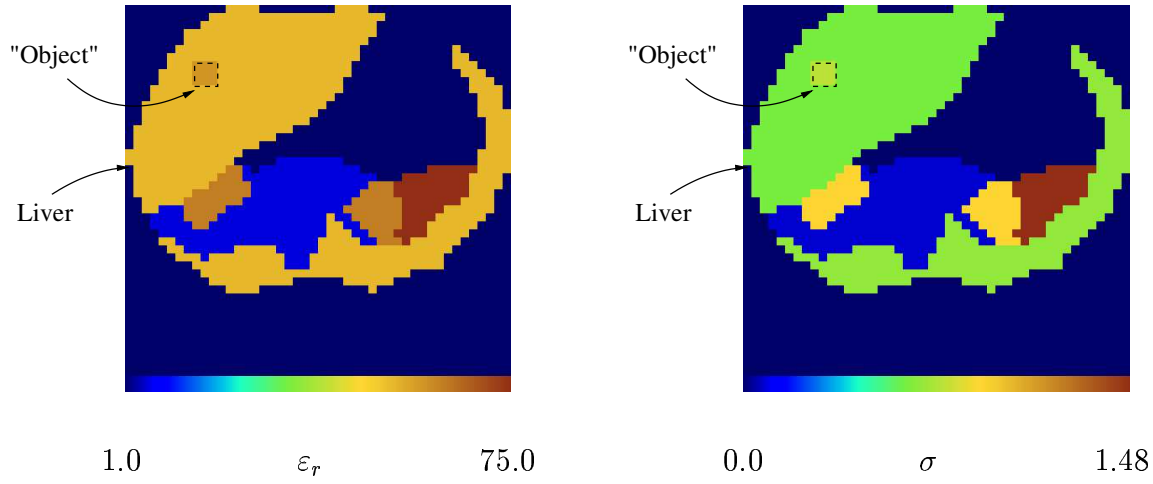

(b)

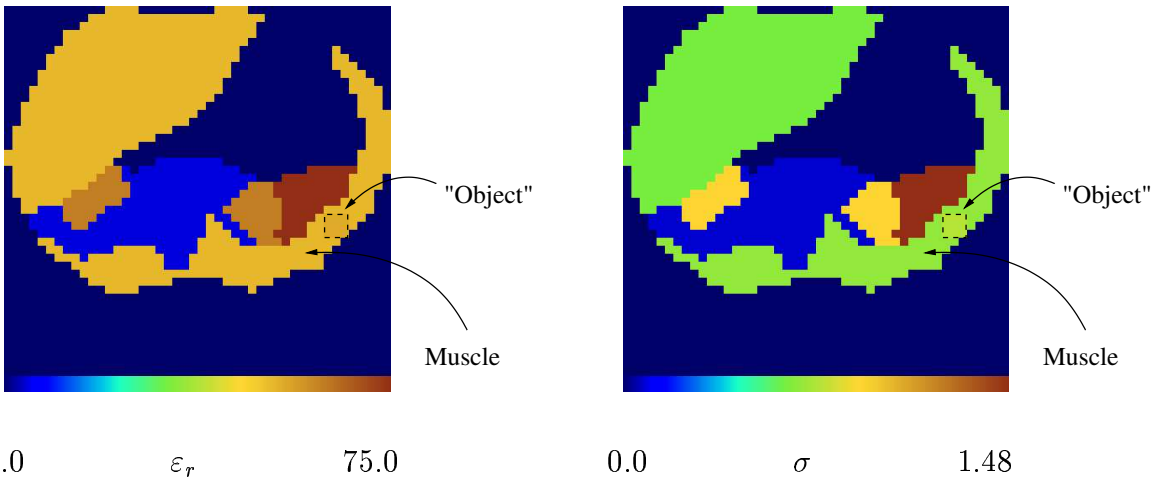

(c)

Fig. 3 - S. Caorsi *et al.*, "Microwave medical imaging: potentialities ..."

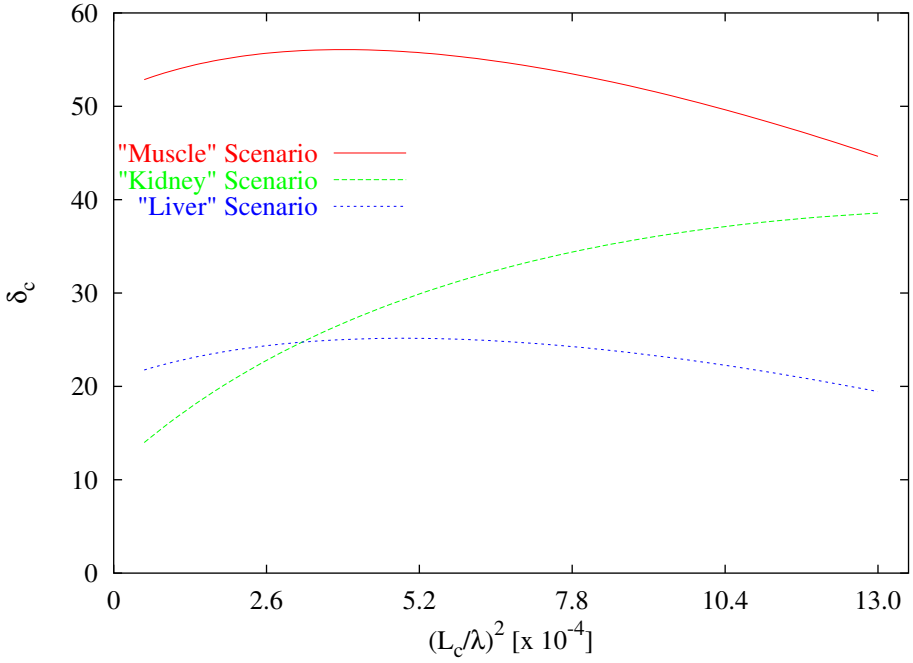

(*a*)

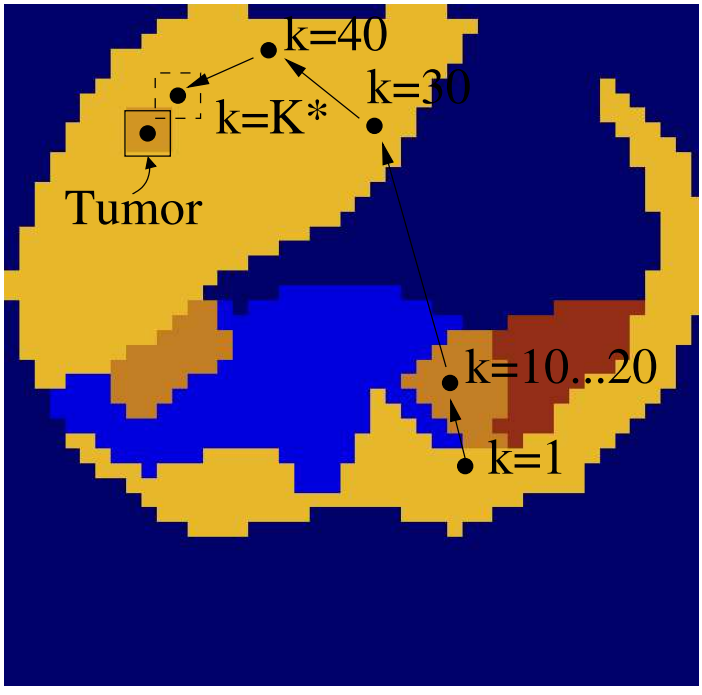

(*b*)

Fig. 4 - S. Caorsi *et al.*, "Microwave medical imaging: potentialities ..."

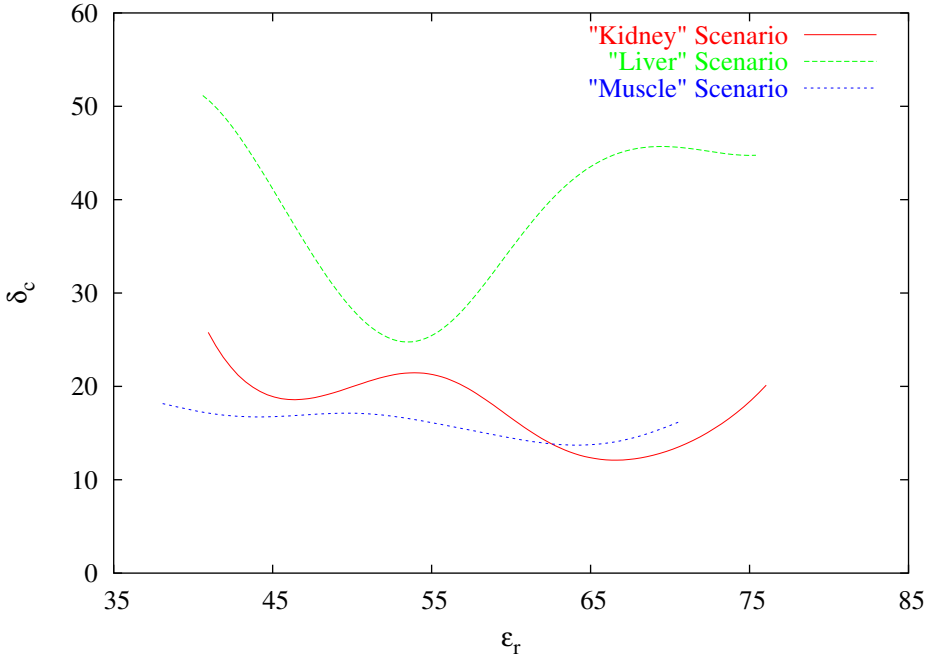

(*a*)

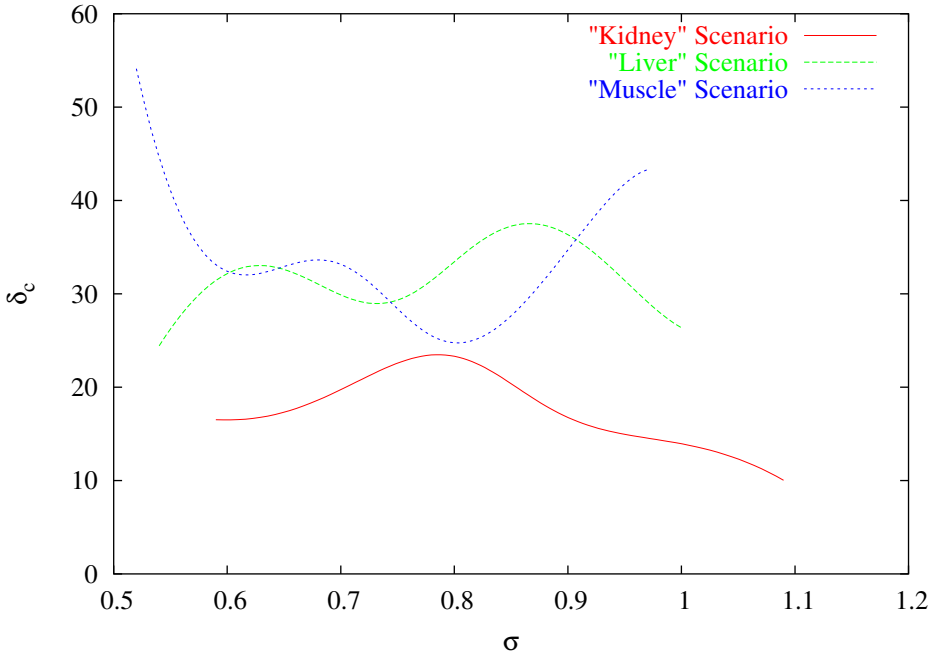

(*b*)

Fig. 5 - S. Caorsi *et al.*, "Microwave medical imaging: potentialities ..."

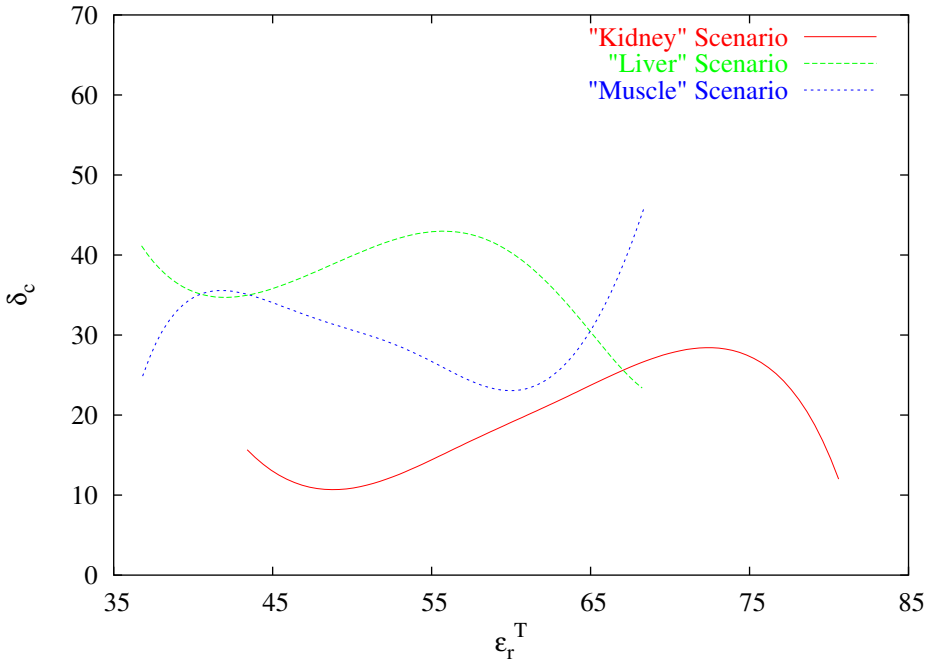

(*a*)

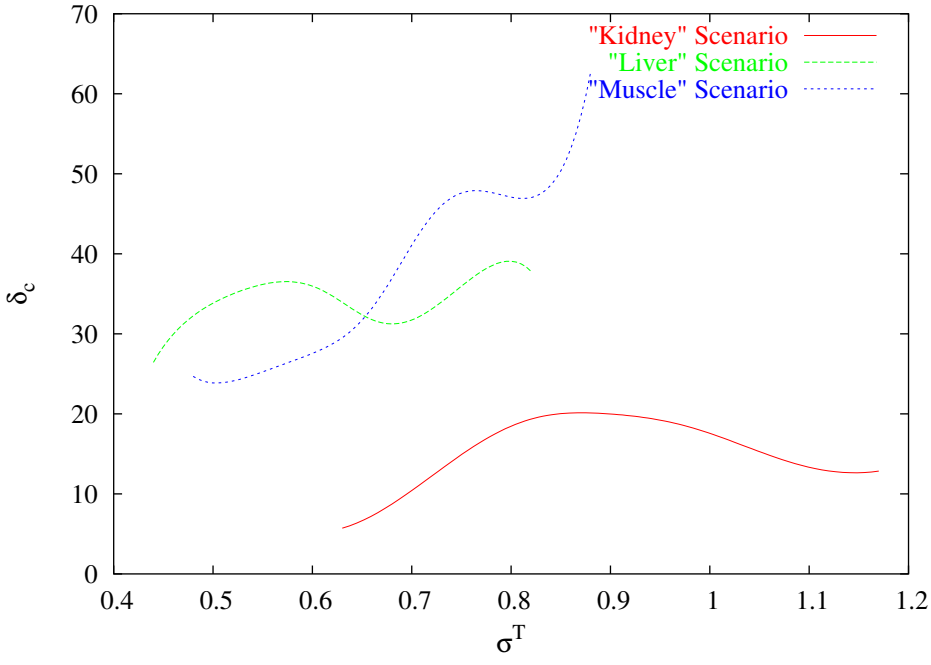

(*b*)

Fig. 6 - S. Caorsi *et al.*, "Microwave medical imaging: potentialities ..."